A DYNAMIC BAYESIAN NETWORK APPROACH FOR DEVICE-FREE RADIO VISION: MODELING, LEARNING AND INFERENCE FOR BODY MOTION RECOGNITION

Stefano Savazzi, Sanaz Kianoush, Vittorio Rampa

National Research Council of Italy (C.N.R.),
Institute of Electronics, Computers and Telecommunication Engineering (I.E.I.I.T.)

ABSTRACT

In this paper, a time-varying dynamic Bayesian network model is shown to describe human-induced RF fluctuations for the purpose of non-cooperative and device-free radio-based body motion recognition (radio vision). The technology relies on pre-existing wireless communication network infrastructures and processes channel quality information (CQI) for human-scale sensing. Body movements leave a characteristic footprint on the CQI sequences collected during consecutive radio transmissions over multiple co-located links. Body-induced RF footprints are proved to be effectively characterized by temporarily coupled hidden Markov chains: abrupt changes of body postures make CQIs observed over co-located links temporarily coupled while being uncoupled for slow body movements. Learning and classification/inference problems are discussed based on experimental measurements. Device-free radio vision performances are evaluated for arm gesture and fall detection applications.

Index Terms— Dynamic Bayesian networks, time-varying HMM, device-free radio vision, activity recognition.

1. INTRODUCTION

Radio vision (RV) systems leverage body-induced diffraction, reflection and scattering phenomena that affect the radio-frequency (RF) propagation for human motion recognition. RV technologies not only allow localization and tracking of people [1][2][3], but also human activity detection [4][5][6]. Body movements are identified and tracked by analyzing the human-induced perturbations of the same RF field generated for wireless data communication, without the need to employ any additional wearable sensor (sensor-free detection), nor to ask for specific user actions (non-cooperative detection). Tracking of human motion and recognition of activities are done through real-time processing of the wireless channel quality information (CQI) over consecutive transmissions. CQI can be either in the form of baseband (BB) radio channel state information (CSI), or received signal strength (RSS) values. RV systems are generally based on the joint processing of specific CQI footprints: in fact, when available, CQIs from multiple links can be combined to improve detection accuracy.

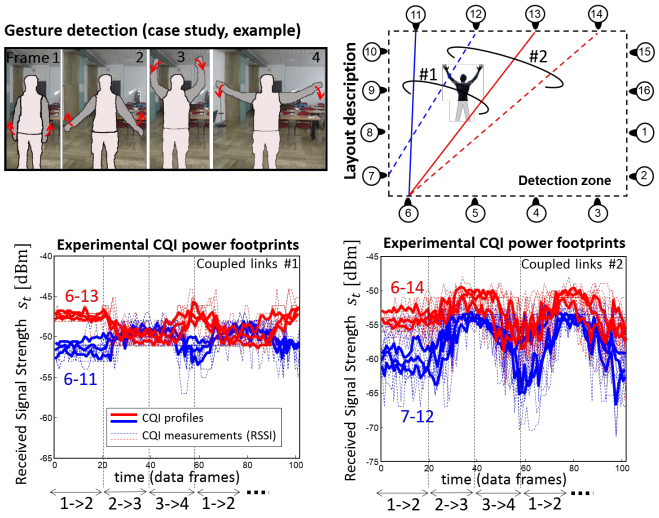

Fig. 1. Wireless network deployment and CQI experimental footprints (RSS) corresponding to a specific arm gesture.

Here, we propose and analyze a novel Dynamic Bayesian Network (DBN) model [7] that can effectively describe the human-induced RF fluctuations and account for spatial (link-wise) correlation of the channel response over multiple links. Analysis of RF measurements reveals that body motions make CQI processes non-stationary, while RF observations over different links might be temporarily coupled due to abrupt changes of body postures, but uncoupled (or weakly coupled) for slow body movements. CQI footprints are thus characterized by coupled Hidden Markov (CHM) chains [8]. Finally, focusing on human activity recognition for assisted living applications [9], learning issues and inference/classification problems are discussed based on experimental measurements.

2. CQI PROCESSING

Let us consider a wireless mesh network whose transmissions are organized into periodic frames, or symbols, and a person

inside the propagation area performing the activity Θ defined as a generic combinations of elementary body motions, with $\Theta = \emptyset$ representing an activity of no interest for recognition purposes, *i.e.,* for human body in free state, or located outside the detection area. The effects of the user state Θ on the channel response are observed over T consecutive received frames (symbols) from which CQI information can be extracted. The CQI (in dB scale) over link ℓ and frame (symbol) $1 \leq t \leq \mathrm{T}$ corresponding to the user state Θ can be modeled as

$$s_t^{(\ell)}(\Theta) = q_t^{(\ell)}(\Theta) + \bar{s}^{(\ell)}(\emptyset) + u_t^{(\ell)}, \tag{1}$$

where $\bar{s}^{(\ell)}(\emptyset) = \mathrm{E}_t\left[s_t^{(\ell)}(\emptyset)\right]$ is the (pre-calibrated) average CQI observed in the human-free state, $q_t^{(\ell)}(\Theta) = \mathrm{E}\left[s_t^{(\ell)}(\Theta) - \bar{s}^{(\ell)}(\emptyset)\right]$ models the body-induced CQI shifts, averaging out background noise term $u_t^{(\ell)}$ caused by: i) measurement errors; ii) effects of environmental changes; iii) time-warping effects as a result of changes in body movement speed, and iv) imperfect body movements. Shifts $q_t^{(\ell)}$ model body-induced shadowing, diffraction [10] and scattering effects (*e.g.,* accounting for arms influence [11]). The sequence of CQI observations $\mathbf{s}_{1:\mathrm{T}}^{(\ell)}(\Theta) = \left\{s_t^{(\ell)}\right\}_{t=1}^{\mathrm{T}}$ acts as human-induced footprint; likewise, the CQI profile $\mathbf{q}_{1:\mathrm{T}}^{(\ell)}(\Theta) = \left\{q_t^{(\ell)}\right\}_{t=1}^{\mathrm{T}}$ highlights the deviations (or shifts) with respect to the human-free state.

Recognition of human activity is commonly based on multi-link processing [4]; Fig. 1 shows the CQI profiles (in terms of RSS) observed over four selected IEEE 802.15.4 links (out of $N = 240$ network links) featuring a person raising and lowering both arms (as depicted in the 4 frames on the top). The RSS shifts, represented here as $q_t^{(\ell)}(\Theta) + \bar{s}^{(\ell)}(\emptyset)$ for comparative analysis with the corresponding RSS observations, are highlighted in solid lines and refer to T=100 consecutive data frames. The profiles have been obtained from 14 RSS measurements $s_t^{(\ell)}(\Theta)$ collected in-lab for all links and correspond to the same repeated gesture (but subject to imperfect body movements and varying motion speed). Links are located at 0.5m above the ground and with layout depicted in the right side. Abrupt changes of body postures, as part of activity Θ (*e.g.,* up/down arm movements: frame 2 to 3 and frame 3 to 4), make the corresponding CQI processes highly time-varying. In particular, CQI shifts extracted from co-located links show substantial correlation in correspondence of fast body movements (*e.g.,* being subject to similar body-induced micro-Doppler effects [12]). On the contrary, for slow body movements (*e.g.,* wandering, standing), RF data-sets are mostly influenced by environmental changes in the surroundings of the link, and thus could be reasonably assumed as marginally correlated. Non-stationarity of CQI processes will be further addressed in the next sections.

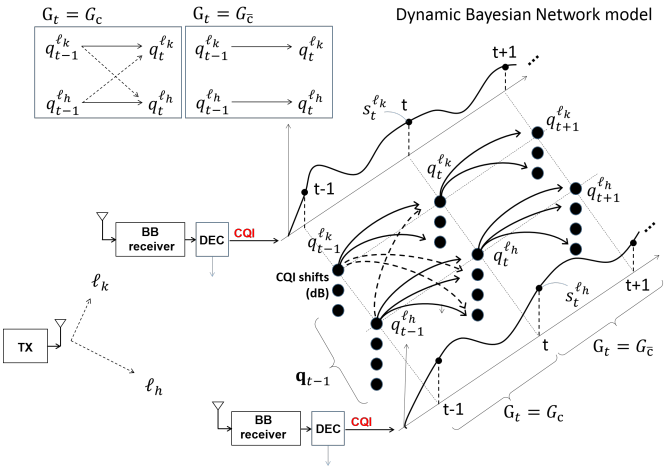

Fig. 2. Dynamic Bayesian network modeling and CQI extraction over two paired wireless links.

3. TIME-VARYING BAYESIAN NETWORK CQI MODELING AND INFERENCE

In what follows, CQI profile terms $\mathbf{q}_{1:\mathrm{T}}^{(\ell)}(\Theta)$ take the role of hidden process states. Moreover, it is: $\mathrm{E}\left[q_t^{(\ell)}|q_{t-1}^{(\ell)}, ..., q_1^{(\ell)}\right] = \mathrm{E}\left[q_t^{(\ell)}|q_{t-1}^{(\ell)}\right]$ since we assume that first-order Markov model-based inference applies. RV systems leverage on dense deployments of devices acting as virtual co-located antennas/links. Therefore, they process multi-dimensional CQI sequences, *i.e.,* $\mathbf{S}_{1:\mathrm{T}} = \left[\mathbf{s}_{1:\mathrm{T}}^{(\ell_1)}(\Theta), ..., \mathbf{s}_{1:\mathrm{T}}^{(\ell_N)}(\Theta)\right]$ acquired from selected link sets $\{\ell_1, ..., \ell_N\}$. A time-varying [7] DBN is proposed here to model the interactions of CQI sequences over multiple links. Hidden CQI shifts are therefore represented in terms of a set of mutually coupled random variables $\mathbf{q}_t(\Theta) = \left[q_t^{(\ell_1)}, ..., q_t^{(\ell_N)}\right]$, that are hidden into the corresponding CQI observations $\mathbf{s}_t = \left[s_t^{(\ell_1)}, ..., s_t^{(\ell_N)}\right]$ as

$$\mathbf{s}_t(\Theta) = \mathbf{q}_t(\Theta) + \bar{\mathbf{s}}(\emptyset) + \mathbf{u}_t \tag{2}$$

with background noise vector $\mathbf{u}_t = \left[u_t^{(\ell_1)}, ..., u_t^{(\ell_N)}\right]$ and the corresponding human-free CQI terms $\bar{\mathbf{s}}(\emptyset)$. The DBN model $\lambda(\Theta)$ consists of: i) a prior network structure G_0 that defines the initial dependency among link states (or nodes) $\Pr\left[\mathbf{q}_0|\mathrm{G}_0\right] = \prod_{k=1}^{N} \Pr\left[q_0^{(\ell_k)}|\mathrm{G}_0\left(q_0^{(\ell_k)}\right)\right]$ with $\mathrm{G}_0(\cdot)$ collecting the parent set of $q_0^{(\ell_k)}$ in the graph and ii) a transition network graph G_t from which the probabilities of each state conditioned on the other variables can be computed as

$$\Pr\left[\mathbf{q}_{t+1}|\mathbf{q}_t, \mathrm{G}_t\right] = \prod_{k=1}^{N} \Pr\left[q_{t+1}^{(\ell_k)}|\mathrm{G}_t\left(q_t^{(\ell_k)}\right)\right]. \tag{3}$$

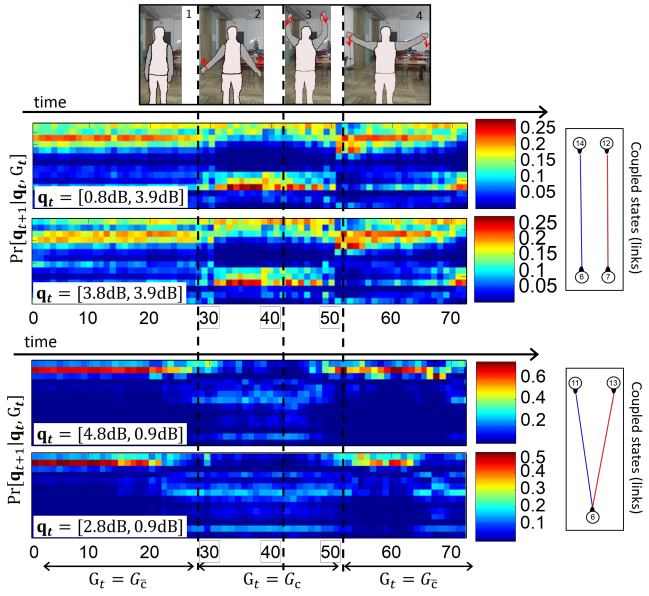

Fig. 3. Time-varying transition probabilities $\Pr\left[\mathbf{q}_{t+1}|\mathbf{q}_t, \mathrm{G}_t\right]$ estimated from training for 2 selected initial states $\mathbf{q}_t$ (with corresponding CQI shifts in dB scale), and for two link pairs:$(6, 14), (7, 12)$ - top - and $(6, 13)$,$(6, 11)$ - bottom. Shift values for joint states $\mathbf{q}_{t+1}$ are omitted to ease visualization.

CQI observation probabilities $\Pr[\mathbf{s}_t|\mathbf{q}_t]$ can be easily trained from data or chosen to account for background measurement noise and possible time-warping effects.

In the following sections, we restrict our attention to time-varying CHM modeling [8]. As depicted in Fig. 2, selected pairs of co-located links $\zeta_{k,h} := (\ell_k, \ell_h)$ are allowed to interact (for some relevant time epochs t) by mutually influencing each other states. Transition network for paired links $\zeta_{k,h}$ can be thus simplified $\forall t$ as G_t:=$\{G_{\mathrm{c}}, G_{\bar{\mathrm{c}}}\}$ to represent coupled $G_{\mathrm{c}}\left(q_t^{(\ell_k)}\right) := \left\{q_t^{(\ell_k)}, q_t^{(\ell_h)}\right\}$, and uncoupled $G_{\bar{\mathrm{c}}}\left(q_t^{(\ell_k)}\right) := \left\{q_t^{(\ell_k)}\right\}$ configurations at epoch t. The (binary) sequence $\mathbf{G}_{1:\mathrm{T}-1} := \{\mathrm{G}_1, ..., \mathrm{G}_{\mathrm{T}-1}\}$ thus rules the time-varying coupling of the embedded CQI shifts.

Considering the coupled link pair $\zeta_{k,h}$, the state transition probability at time epoch t is $\Pr\left[\mathbf{q}_{t+1}|\mathbf{q}_t, \mathrm{G}_t = G_{\mathrm{c}}\right] = a^{(\ell_k)}_{m|n,q} \times a^{(\ell_h)}_{p|n,q}$ with $a^{(\ell_k)}_{m|n,q} = \Pr\left[q^{(\ell_k)}_{t+1} = \mathrm{q}_m|\mathbf{q}_t = \mathbf{q}_{n,q}\right]$ and $\mathbf{q}_{n,q} = \left[q_t^{(\ell_k)} = \mathrm{q}_n, q_t^{(\ell_h)} = \mathrm{q}_q\right]$. The same considerations apply also to $a^{(\ell_h)}_{p|n,q}$. For uncoupled epochs $\Pr\left[\mathbf{q}_{t+1}|\mathbf{q}_t, \mathrm{G}_t = G_{\bar{\mathrm{c}}}\right] = a^{(\ell_k)}_{m|n} \times a^{(\ell_h)}_{p|q}$ with straightforward definitions. For the same example summarized in Fig. 1, Fig. 3 shows the time-varying transition probability functions (3) estimated from training data-sets for 2 selected initial states and link pairs. The highlighted epochs correspond to coupled/uncoupled states: in particular, it can be shown that coupled states are mostly induced by fast up/down movements of the arms.

Likelihood evaluation for activity classification is based on the forward-backward algorithm (*i.e.,* frontier method [13]): the joint probability $\Pr\left[\mathbf{S}_{1:\mathrm{t}}, \mathbf{q}_t = \mathbf{q}_{n,q}|\mathbf{G}_{1:t-1}\right] = \alpha_t(\mathbf{q}_{n,q}|\mathbf{G}_{1:t-1})$ is iteratively evaluated for $0 \leq t \leq \mathrm{T}-1$ and accounts for time-varying coupled states as

$$\alpha_{t+1}\left(\mathbf{q}_{t+1} = \mathbf{q}_{m,p}|\mathbf{G}_{1:t}\right) = \Pr\left(\mathbf{s}_{t+1}|\mathbf{q}_{m,p}\right) \times \times \sum_{\mathbf{q}_{n,q}} \alpha_t\left(\mathbf{q}_{n,q}|\mathbf{G}_{1:t-1}\right) \times a^{(\ell_k)}_{m|n,q} a^{(\ell_h)}_{p|n,q} \tag{4}$$

with $\alpha_0\left(\mathbf{q}_0\right) = \Pr\left[\mathbf{q}_0|\mathrm{G}_0\right]$. The likelihood function used for classification is $\Pr\left[\mathbf{S}_{1:\mathrm{T}}|\lambda\right] = \sum_{\mathbf{q}_\mathrm{T}} \alpha_\mathrm{T}(\mathbf{q}_\mathrm{T}|\mathbf{G}_{1:\mathrm{T}-1})$ while the decision on activity $\widehat{\Theta}$ over the link pair $\zeta_{k,h}$ is taken if $\Gamma_{\zeta_{k,h}}(\Theta) \geq \tau$ with log-likelihood rate $\Gamma_{\zeta_{k,h}}(\Theta) = \ln\frac{\Pr[\mathbf{S}_{1:\mathrm{T}}|\lambda(\Theta)]}{\Pr[\mathbf{S}_{1:\mathrm{T}}|\lambda(\emptyset)]}$ and major voting over the selected link pairs. Model $\lambda(\emptyset)$ for human-free state is given by standard HMM and trained with CQI data corresponding to random body movements in the same area. Varying threshold τ, analyzed in Sect. 5, defines the detector receiver operating characteristic (ROC) points and achievable sensitivity/false positive rates.

4. DBN MODEL: LEARNING AND TRAINING

Expectation-Maximization (EM) algorithm can be applied to locally maximize the model likelihood through an iterative procedure. Starting from a DBN model estimate $\lambda^{(j)}$ at iteration j, it evaluates the time-varying (a-posteriori) probabilities of state occurrence/transition, given the new observed sequence $\bar{\mathbf{S}}^{(j+1)}_{1:\mathrm{T}}$ for activity Θ. These probabilities are then used to reestimate the DBN parameter set $\lambda^{(j+1)}$ such that $\Pr\left[\bar{\mathbf{S}}^{(j+1)}_{1:\mathrm{T}}|\lambda^{(j+1)}\right] \geq \Pr\left[\bar{\mathbf{S}}^{(j+1)}_{1:\mathrm{T}}|\lambda^{(j)}\right]$, while the procedure stops when some limiting criterion on convergence is met. In what follows, we focus on learning of time-varying transition network and states $a^{(\ell_k)}_{m|n,q}(j+1)$, $a^{(\ell_h)}_{p|n,q}(j+1)$, while reestimation of initial state and observation probability can be easily extended following standard Baum-Welch method [8].

Let us define, for step j, the state transition probabilities $a^{(\ell_k)}_{m|n,q}(j)$, $a^{(\ell_h)}_{p|n,q}(j)$, and, for the new step $j+1$, the binary sequence of transition networks $\mathbf{G}^{(j+1)}_{1:\mathrm{T}-1} := \{\mathrm{G}_1, ..., \mathrm{G}_{\mathrm{T}-1}\}$, reestimation of probability terms $a^{(\ell_k)}_{m|n,q}(j+1)$, $a^{(\ell_h)}_{p|n,q}(j+1)$ from step j is based on $\xi_{t,\mathrm{c}} = \Pr\left[\mathbf{q}_{t+1}, \mathbf{q}_t|\bar{\mathbf{s}}_t, \mathrm{G}^{(j+1)}_t = G_{\mathrm{c}}, \lambda^{(j)}\right]$

$$\xi_{t,\mathrm{c}}\left(\mathbf{q}_{m,p}, \mathbf{q}_{n,q}\right) = \frac{\alpha_t\left(\mathbf{q}_{n,q}|\mathbf{G}^{(j+1)}_{1:t-1}\right) a^{(\ell_k)}_{m|n,q}(j) a^{(\ell_h)}_{p|n,q}(j)}{\Pr\left[\bar{\mathbf{S}}^{(j+1)}_{1:\mathrm{T}}|\lambda^{(j)}\right]} \times \times \Pr\left(\bar{\mathbf{s}}_t|\mathbf{q}_{n,q}\right) \beta_{t+1}\left(\mathbf{q}_{m,p}|\mathbf{G}^{(j+1)}_{t+1:\mathrm{T}-1}\right) \tag{5}$$

with backward equation β_t= $\Pr\left[\bar{\mathbf{S}}^{(j+1)}_{t+1:\mathrm{T}}|\mathbf{q}_t = \mathbf{q}_{m,p}, \mathbf{G}^{(j+1)}_{t+1:\mathrm{T}-1}\right]$ iteratively computed as in (4). Given the joint state probabili-

ties $\pi_{t,c}(\mathbf{q}_{n,q}) = \sum_{m,p} \xi_{t,c}(\mathbf{q}_{m,p}, \mathbf{q}_{n,q})$, finally it is

$$a_{m|n,q}^{(\ell_k)}(j+1) = \frac{\sum_{\forall t|\mathrm{G}_t=G_c} \sum_p \xi_{t,c}(\mathbf{q}_{m,p}, \mathbf{q}_{n,q})}{\sum_{\forall t|\mathrm{G}_t=G_c} \pi_{t,c}(\mathbf{q}_{n,q})}. \quad (6)$$

The corresponding terms $a_{m|n}^{(\ell_k)}(j+1)$, $a_{p|q}^{(\ell_h)}(j+1)$ for uncoupled time epochs $\mathrm{G}_t^{(j+1)} = G_{\bar{c}}$ are not shown but straightforwardly defined given $\xi_{t,\bar{c}}$ and $\pi_{t,\bar{c}}(\mathbf{q}_{n,q}) = \sum_{m,p} \xi_{t,\bar{c}}(\mathbf{q}_{m,p}, \mathbf{q}_{n,q})$. Finally, reestimation of the binary sequence $\mathbf{G}_{1:\mathrm{T}-1}^{(j+1)}$ based on $\mathbf{G}_{1:\mathrm{T}-1}^{(j)}$ can be found by exhaustive search as

$$\begin{aligned} \mathbf{G}_{1:\mathrm{T}-1}^{(j+1)} &= \arg\min_{\forall \mathbf{G}_{1:\mathrm{T}-1}} \left\| \mathbf{G}_{1:\mathrm{T}-1} - \mathbf{G}_{1:\mathrm{T}-1}^{(j)} \right\| \quad (7) \\ \text{s.t.} &\Pr\left[\bar{\mathbf{S}}_{1:\mathrm{T}}^{(j+1)} | \lambda^{(j+1)}\right] \geq \Pr\left[\bar{\mathbf{S}}_{1:\mathrm{T}}^{(j+1)} | \lambda^{(j)}\right] \end{aligned}$$

with norm $\|\cdot\|_2$. Eq. (7) is chosen to guarantee stability of the solution with respect to the initial sequence $\mathbf{G}_{1:\mathrm{T}-1}^{(0)}$.

5. EXPERIMENTAL VALIDATION

The proposed DBN model is validated through extensive experimental measurements, focusing on arm gesture recognition (Fig. 1) and detection of impact shock during fall event. Gesture detection measurements are obtained from two human targets with different body structures but placed at the same location (estimated through localization methods [2] [3]). For fall detection, training data-sets are obtained for target falling at different directions *i.e.,* front, rear, left and right. The corresponding channel quality measurements are obtained from 16 IEEE 802.15.4 standard-compliant RF nodes randomly deployed in the surrounding of the target and processing RSS measurements as CQI data. In what follows, we compare the detection performance of the proposed model against the ones obtained with the plain HMM-based single link model [14]. Fig. 4.a and Fig. 4.b show the gesture (DR) and non-gesture (NR) detection ratios for all 240 uncoupled links (left), and for a selection of 182 pairs of coupled links (right), respectively. The proposed DBN approach jointly takes into account the correlation of CQIs over paired links and the non-stationarity of the data-sets due to fast body movements. Compared with the single-link approach Fig. 4.a, characterized by an experimental average DR-NR separation of 8 dB, the DBN model-based detector of Fig. 4.b guarantees an average separation greater than 86 dB.

The ROC curves for fall detection (red lines) and arm gesture recognition (blue lines) compare the sensitivity vs. the false positive rate of the detector: the results are depicted in Fig. 5 based on a complete set of 4326 measurements from the single links and 11284 measurements from the paired links. The solid lines highlight the performances of the proposed DBN-based detector while the dashed lines correspond to the single link HMM-based detector case. Focusing on fall detection, the use of paired links for detection guarantees a sensitivity up to 0.994 with corresponding false positive rate of

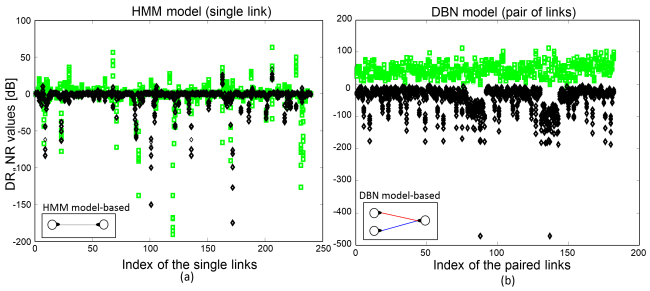

Fig. 4. DR and NR likelihood ratios for arm gesture recognition, corresponding to (a) 240 HMM-based values over single links and (b) DBN-based ones over 182 pair of links.

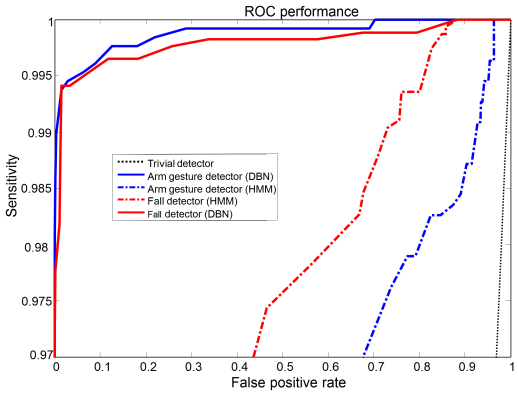

Fig. 5. ROC curve for fall detection (red line) and arm gesture detection (blue line) using single link HMM-based detection (dashed lines) and time-varying DBN-based (solid lines) methods.

about 0.01 that is well aligned with existing sensor-based devices [15]. On the contrary, for HMM-based detector, achievable sensitivity for the same false positive rate drops down to 0.75. These results are obtained at the expense of an increased computational complexity with respect to the uncoupled links case. However, the adoption of a major voting strategy over an optimized subset of links (not considered here) would provide additional performance and computational complexity improvements in both cases.

6. CONCLUSIONS

The paper proposes the use of DBN-based techniques for device-free radio vision systems. The DBN model describes the human-induced CQI footprints, and account for non-stationarity and spatial (link-wise) correlation of the channel response over multiple links. The proposed model is validated for human body motion recognition through extensive experimental RF measurements, focusing on arm gesture recognition and fall detection. Detection performance is analyzed in terms of sensitivity and false positive rates.

7. REFERENCES

[1] J. Wilson and N. Patwari, "Radio tomographic imaging with wireless networks," *IEEE Transactions on Mobile Computing*, vol. 9, no. 5, pp. 621–632, May 2010.

[2] A. Saeed, A.E. Kosba, and M. Youssef, "Ichnaea: A low-overhead robust wlan device-free passive localization system," *IEEE Journal of Selected Topics in Signal Processing*, vol. 8, no. 1, pp. 5–15, Feb 2014.

[3] S. Savazzi, M. Nicoli, F. Carminati, and M. Riva, "A Bayesian approach to Device-Free Localization: Modeling and experimental assessment," *IEEE Journal of Selected Topics in Signal Processing*, vol. 8, no. 1, pp. 16–29, Feb 2014.

[4] S. Shi, M. Scholz, M. Beigl, Y. Ji, and S. Sigg, "Rf-sensing of activities from non-cooperative subjects in device-free recognition systems using ambient and local signals," *IEEE Transactions on Mobile Computing*, vol. 13, no. 4, pp. 907–920, 2014.

[5] N. Patwari, L. Brewer, Q. Tate, O. Kaltiokallio, and M. Bocca, "Breathfinding: A wireless network that monitors and locates breathing in a home," *IEEE Journal of Selected Topics in Signal Processing*, vol. 8, no. 1, pp. 30–42, Feb 2014.

[6] B. Mager, N. Patwari, and M. Bocca, "Fall detection using rf sensor networks," in *IEEE 24th International Symposium on Personal Indoor and Mobile Radio Communications (PIMRC)*, Sept 2013, pp. 3472–3476.

[7] Zhaowen Wang, E.E. Kuruoglu, Xiaokang Yang, Yi Xu, and T.S. Huang, "Time varying dynamic bayesian network for nonstationary events modeling and online inference," *IEEE Transactions on Signal Processing,*, vol. 59, no. 4, pp. 1553–1568, April 2011.

[8] S.M. Chu and T.S. Huang, "An experimental study of coupled hidden markov models," in *IEEE International Conference on Acoustics, Speech, and Signal Processing (ICASSP)*, May 2002, vol. 4, pp. 4100–4103.

[9] S. Savazzi, S. Sigg, M. Nicoli, V. Rampa, S. Kianoush, and U. Spagnolini, "Radio vision for assisted living: leveraging wireless channel quality information for human sensing," *IEEE Signal Processing Magazine*, March 2016, in press.

[10] V. Rampa, S. Savazzi, M. Nicoli, and M. D'Amico, "Physical modeling and performance bounds for device-free localization systems," *IEEE Signal Processing Letters,*, vol. 22, no. 11, pp. 1864–1868, Nov 2015.

[11] R. Chandra and A.J. Johansson, "An analytical link-loss model for on-body propagation around the body based on elliptical approximation of the torso with arms' influence included," *IEEE Antennas and Wireless Propagation Letters,*, vol. 12, pp. 528–531, 2013.

[12] K.Youngwook and L. Hao, "Human activity classification based on micro-doppler signatures using a support vector machine," *IEEE Transactions on Geoscience and Remote Sensing,*, vol. 47, no. 5, pp. 1328–1337, May 2009.

[13] J. Bilmes and G. Zweig, "The graphical models toolkit: An open source software system for speech and time-series processing," in *IEEE International Conference on Acoustics, Speech, and Signal Processing (ICASSP)*, May 2002, vol. 4, pp. 3916–3919.

[14] S. Kianoush, S. Savazzi, F. Vicentini, V. Rampa, and M. Giussani, "Leveraging rf signals for human sensing: fall detection and localization in human-machine shared workspaces," in *Proc 13th IEEE International Conference on Industrial Informatics (INDIN), Cambridge, U.K.*, July 2015.

[15] R. Igual, M. Carlos, and P. Inmaculada, "Challenges, issues and trends in fall detection systems," *BioMedical Engineering OnLine*, vol. 12, no. 1, pp. 66, 2013.